

# Smart Supramolecular Sensing with Cucurbit[*n*]urils: Probing Hydrogen Bonding with SERS

B. de Nijs,<sup>a</sup> M. Kamp,<sup>b</sup> I. Szabó,<sup>c</sup> S. J. Barrow,<sup>b</sup> F. Benz,<sup>a</sup> G. Wu,<sup>b</sup> C. Carnegie,<sup>a</sup>  
R. Chikkaraddy,<sup>a</sup> W. Wang,<sup>a</sup> W. M. Deacon,<sup>a</sup> E. Rosta,<sup>c</sup> J. J. Baumberg<sup>a</sup> and O. A. Scherman<sup>b</sup>

## Supplementary Information

---

<sup>a</sup> NanoPhotonics Centre, Cavendish Laboratory, University of Cambridge, Cambridge CB3 0HE, UK.

<sup>b</sup> University of Cambridge, Melville Laboratory for Polymer Synthesis, Department of Chemistry, Cambridge CB2 1EW, UK.

<sup>c</sup> King's College London, Department of Chemistry, London, UK.

† Correspondence should be addressed to [bd355@cam.ac.uk](mailto:bd355@cam.ac.uk) or [oas23@cam.ac.uk](mailto:oas23@cam.ac.uk).

# 1. Additional Experimental Results

## Control measurements

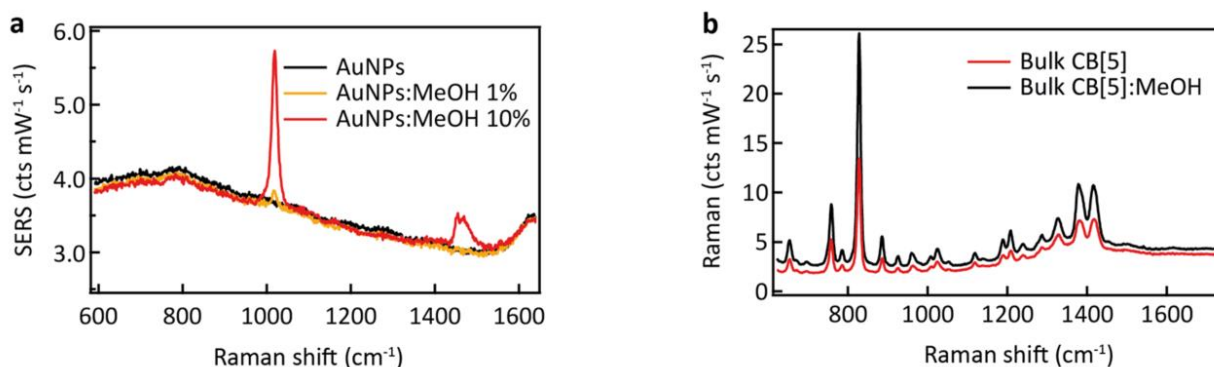


Figure S1: MeOH control measurements. **a)** Raman spectrum of AuNPs with 1-10 % MeOH added showing only peaks at  $1018\text{ cm}^{-1}$  and  $1450\text{ cm}^{-1}$ . **b)** Bulk Raman spectrum of CB[5] with MeOH added showing no clear change in the spectrum.

## CB[6] with MeOH

Gradually increasing the amount of MeOH in CB[6]-AuNPs shows a similar trend to that observed for MeOH in CB[5] aggregates. However, if we look closely at the peak position for CB[6] we see they match more closely to the observed spectrum for EtOH in CB[5] with peak position at  $1539\text{ cm}^{-1}$  and  $1604\text{ cm}^{-1}$ .

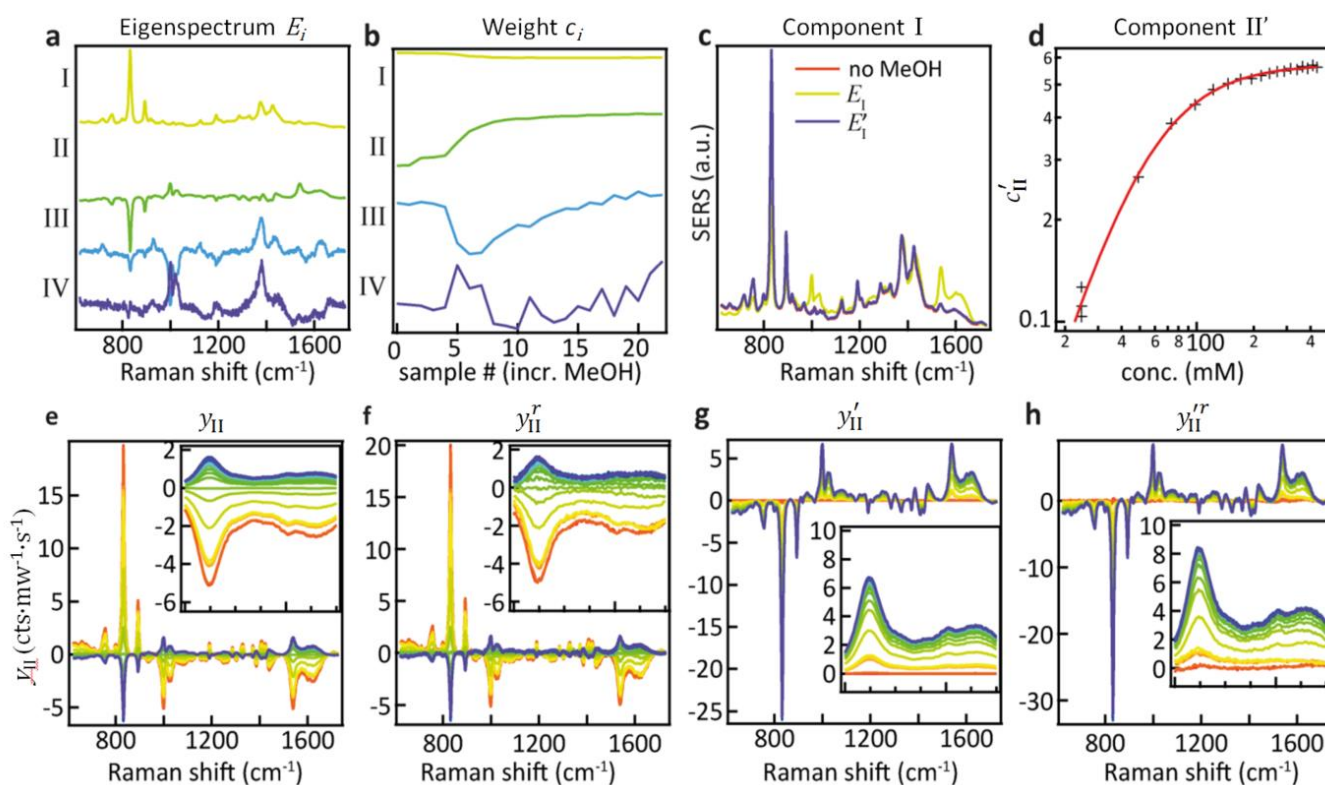


Figure S2: Principal component analysis of spectral changes in CB[6]-AuNP aggregates upon addition of MeOH. **a)** The first four component eigenspectra  $E_i$ . **b)** Weights (PCA score)  $c_i$  for each of the components showing their variation upon addition of MeOH from 0-500mM. **c)** Comparison of  $E_I$ ,  $E_I'$  and a pure CB[6] spectrum. **d)** The weights  $c'_{II}$  of PC II plotted against MeOH concentration showing clear correlation. **e)** Plot showing  $E_{II}$  multiplied by its weights  $c_{II}$  highlighting the changes upon addition of MeOH. **f)** Reconstituted change in PC II, obtained by subtracting  $y_{I,III-VI}$  from the raw dataset. **g, h)** Same plots as e, f but with the weight offset by its value at  $m=0$  v/v% MeOH, showing the reconstructed spectral changes for PC II. The dotted line in the inset is the bulk Raman signal of MeOH in this region.

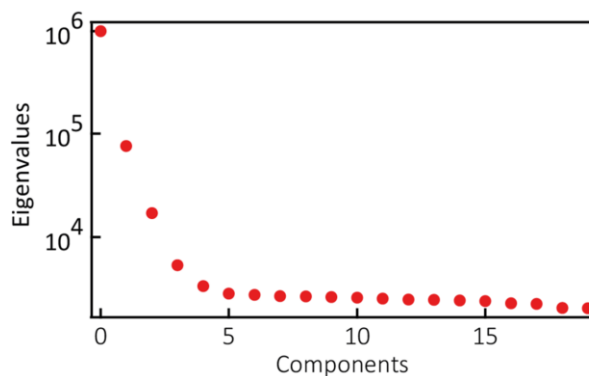


Figure S3: Typical weights for each of the PCA components, here obtained for the CB[5] with MeOH concentration series. This shows the first three components are the most relevant with rapidly diminishing contributions for the remaining components.

## 2. Principle Component Analysis (PCA)

The Wavemetrics Igor implementation of principal component analysis was used, which is based on [1]. No smoothing or normalisation is applied to the dataset prior to analysis. Before analysis the datasets are normalised by the laser power in mW and the integration time in seconds resulting in counts  $\text{mW}^{-1}\text{s}^{-1}$  for the intensity.

## 3. Computational Details

We have carried out gas phase geometry optimisations and subsequent frequency calculations for the  $\text{H}_2\text{O}$ , MeOH, EtOH ligands and the  $\text{H}_2\text{O}:\text{H}_2\text{O}$ ,  $\text{H}_2\text{O}:\text{MeOH}$ ,  $\text{H}_2\text{O}:\text{EtOH}$  binary complexes employing density functional theory (DFT) with the hybrid B3LYP exchange-correlation energy functional in combination with the correlation-consistent polarized valence triple- $\zeta$  basis sets augmented with diffuse functions, aug-cc-pVTZ basis set. Gas phase geometry optimisations and frequency computations for CB[5] and CB[5]:Ligand (Ligand = MeOH, EtOH,  $\text{H}_2\text{O}$ ,  $\text{N}_2$  and  $\text{O}_2$ ) were performed using the DFT B3LYP method in combination with the split-valence double-zeta polarized basis set, 6-31G\* and including the Grimme's D3 dispersion correction with Becke-Jonhson damping.<sup>[2]</sup> All standard DFT computations were performed by the Gaussian 09<sup>[3]</sup> ab initio program package. Raman shifts were obtained by scaling the ab initio frequencies with the empirical factors of 0.968 and 0.960 corresponding to the B3LYP/aug-cc-pVTZ and B3LYP-D3/6-31G\* levels of theory, respectively. Finally, the Raman spectra were obtained by applying Lorentzian broadening with bandwidth at half height of  $20\text{cm}^{-1}$ .

Association free energies were calculated following Grimme et al.<sup>[4]</sup> Accordingly, gas phase geometry optimisations of the complexes (CB[5]:MeOH/EtOH), host(CB[5]) and guest (MeOH/EtOH) molecules were performed using B3LYP functional in combination with the Def2TZVP basis set and including the Grimme's D3 dispersion correction with Becke-Johnson damping<sup>[2]</sup>. Frequency calculations were performed at the same level of theory to obtain the thermostatical corrections from energy to free energy in the rigid rotor/harmonic-oscillator approximation and including zero-point vibrational energy in the gas phase at 298K and 1 atm ( $G_{\text{RRHO}}^T$ ). Solvation free energy was obtained at the same level of theory and using SMD ( $G_{\text{SMD}}$ ) and PCM ( $G_{\text{PCM}}$ ) continuum solvent models. Association free energy ( $\Delta G_a$ ) is then calculated as the sum of those contributions to the gas phase association energy  $\Delta E$ :

$$\Delta G_a = \Delta E + \Delta G_{\text{RRHO}}^T + \Delta G_{\text{SMD/PCM}}$$

The  $\Delta$  symbol represents that the supramolecular approach  $\Delta X = X(\text{complex}) - X(\text{host}) - X(\text{guest})$  have been used. The association free energies are summarized in Table S1.

Molecular dynamics (MD) simulations were performed with the NAMD 2.9<sup>[5]</sup> program using the CHARMM36<sup>[6]</sup> force field. The force field parameters for CB[n], n=5,6 were generated with the CGenFF program.<sup>[7]</sup> The CB[5] cage containing the MeOH/EtOH ligands and the CB[6] cage with MeOH were solvated with a pre-equilibrated TIP3 cubic water box of edge 50

and 60 Å, respectively. The resulting systems contain 11712, 11727 and 20487 atoms for CB[5]:MeOH, CB[5]:EtOH and CB[6]:MeOH, respectively. Our MD protocol consisted of: (1) equilibration including energy minimization of the CB[n]:MeOH ( $n=5,6$ ) and CB[5]:EtOH systems over 1 ns in the NVT ensemble, (2) umbrella sampling production runs of 5 ns in the NPT ensemble for each 48 windows with a spring constant of 100 and 75 kcal/(mol Å<sup>2</sup>) for CB[5]:MeOH/EtOH and CB[6]:MeOH, respectively. A time step of 2 fs was used. Temperature and pressure were held constant at 303.15 K and 1 atm, respectively. All of the bonds and angles involving hydrogen atoms were constrained by the SHAKE<sup>[8]</sup> algorithm. We used the particle mesh Ewald method<sup>[9]</sup> for the long-range electrostatics in combination with a 12 Å cutoff for the evaluation of the non-bonded interactions. The umbrella bias for the host-guest association process was defined as the distance between center of mass of CB[n],  $n=5,6$  oxygen atoms on one side of the cage and the center of mass of the MeOH/EtOH ligands. We used the dynamic histogram analysis method (DHAM)<sup>[10]</sup> to compute the free energy profiles along the association coordinate. The final free energy profiles shown on Figure 4b were obtained by shifting the profiles obtained with DHAM to the center of mass of CB[n],  $n=5,6$  (see also Figure 4a).

#### 4. Supplementary Computational Results

Table S1: Association free energies for the CB[5]:MeOH/EtOH complexes in kcal mol<sup>-1</sup> using continuum solvent models.

	$\Delta G_a(\text{SMD})$	$\Delta G_a(\text{PCM})$
CB[5]:MeOH (in)	-0.7	-2.4
CB[5]:MeOH (out <sub>1</sub> )	2.3	2.8
CB[5]:MeOH (out <sub>2</sub> )	4.5	3.7
CB[5]:EtOH (in)	4.9	2.5
CB[5]:EtOH (out <sub>1</sub> )	2.6	3.9
CB[5]:EtOH (out <sub>2</sub> )	5.2	4.3

#### 5. Supplementary Fit Results

Table S2: Hill-Langmuir fit parameters.

	$K_D$	Hill coef. ( $n$ )	$n_{\text{max}}$
CB[5]:MeOH	140	2.0	0.7
CB[6]:MeOH	51	1.9	0.6
CB[5]:EtOH	56	0.9	1.0

#### 6. Supplementary References

- [1] E. R. Malinowski, *Factor Analysis in Chemistry*, John Wiley and Sons, New York, 2nd ed., 1991.
- [2] S. Grimme, S. Ehrlich, L. J. Goerigk, *J Comp Chem*, 2011, **32**, 1456.
- [3] M. J. Frisch et al., Gaussian 09, revision E01; Gaussian, Inc.: Wallingford, CT, 2009.
- [4] R. Sure, S. Grimme, *J Chem Theory Comput*, 2015, **11**, 3785.
- [5] J. C. Phillips, R. Braun, W. Wang, J. Gumbart, E. Tajkhorshid, E. Villa, C. Chipot, R. D. Skeel, L. Kalé, K. J. Schulten, *J Comput Chem*, 2005, **26**, 1781.
- [6] J. Huang, A. D. J. MacKerell, *J Comput Chem*, 2013, **34**, 2135.
- [7] K. Vanommeslaeghe et al., *J. Comput. Chem.* 2010, **31**, 671.
- [8] H. C. J. Andersen, *J Comput Phys*, 1983, **52**, 24.
- [9] T. Darden, D. York, L. J. Pedersen, *J Chem Phys*, 1993, **98**, 10089.
- [10] E. Rosta, G. J. Hummer, *J Chem Theory Comput*, 2015, **11**, 276.